Available online at www.sciencedirect.com
SCIENCE DIRECT®
Ultramicroscopy ▮ (▮▮▮▮) ▮▮▮–▮▮▮
ELSEVIER
ultramicroscopy
-www.elsevier.com/locate/ultramic

Rapid structure determination of a metal oxide from pseudo-kinematical electron diffraction data

C.S. Own[a,*], W. Sinkler[b], L.D. Marks[a]

[a]*Department of Materials Science, Northwestern University, 2220 Campus Dr., Cook 2036, Evanston, IL 60208, USA*
[b]*UOP LLC, Des Plaines, IL 60017, USA*

Received 15 April 2005; received in revised form 13 June 2005; accepted 22 June 2005

Abstract

The electron precession diffraction technique is employed to provide quasi-kinematical data for determination of atom positions in the $(Ga,In)_2SnO_5$ *m*-phase. Precession data are compared with conventional diffraction data captured under identical conditions and show a distinct superiority because they exhibit kinematical characteristics in the structure-defining reflections. Precessed data are not usable within a kinematical interpretation in all cases, and a simple basis is presented for omission of errant reflections to improve adherence to kinematical behavior. A second approach is demonstrated where intensities are used with direct methods instead of amplitudes, enhancing the contrast between strong and weak beams. The unrefined atom positions recovered a priori via direct methods are consistent between the two approaches and fall on average within 4 picometers of positions in the previously refined structure.

PACS: 61.14.Dc; 61.14.Lj; 61.66.Fn

Keywords: Electron diffraction; Electron precession; Direct methods; Crystallography

1. Introduction

Many current crystallography problems require nanoprobe techniques to investigate the length scale of interest. These include precipitate studies, bulk catalyst supports, and surface studies. The transmission electron microscope (TEM) is one tool that is particularly suitable for nanoprobe studies, simultaneously providing imaging and diffraction modes plus chemical probes within a self-contained laboratory system. For investigations of unknown structures, it has proven to be limited in studying thick specimens or specimens containing heavy elements due to distortion of diffraction data and images by multiple scattering. Progress in this area is steadily being made and

*Corresponding author. Tel.: +1 847 491 7809; fax: +1 847 491 7820.
E-mail address: csown@northwestern.edu (C.S. Own).

0304-3991/$ - see front matter © 2005 Elsevier B.V. All rights reserved.
doi:10.1016/j.ultramic.2005.06.058

several powerful tools are now available to solve structures using the electron microscope. New experimental techniques and development of software suites in recent years (and better understanding of what is required for them to work [1]) has yielded successful solution of previously intractable complex structures. Direct imaging of lattice projections using sub-Å probes has been accomplished on irradiation-resistant materials with aberration-corrected scanning microscopes, and point resolution in phase contrast images from corrected TEMs is of similar order [2,3]. Reciprocal space approaches include:

- use of kinematical crystallography algorithms (e.g., Sir97) on dynamical data [4,5] or modifications of dynamical data [6],
- use of kinematical algorithms with data carefully collected to be as kinematical as possible (e.g., surfaces) [7,8],
- dynamical algorithms that refine existing structure models to account for dynamical effects [9,10],
- combinations of the above.

Of these, the precession diffraction technique has been shown to be useful in improving data quality by making intensities more kinematical [11]. Precession electron diffraction (PED) utilizes a serially generated hollow illumination cone with tilt semi-angle typically less than 50 mrad ($\sim 3^\circ$, or $<2\,\text{Å}^{-1}$ at 200 kV) which is combined with a complementary post-specimen descan to bring the scattered beams to measurable spots. It has been employed in the solution of two unknown structures, in one study using precession intensities alone [12], and in two others utilizing a forward dynamical calculation employing some known structure factors to correct intensities [13,14]. In this note, a case is demonstrated wherein a metal oxide structure known to be a strongly dynamical scatterer yields a direct solution without phase information or modification of experimental intensity values.

The Ga–In–Sn–O ternary oxide system (GITO) was previously investigated for use as a potential transparent conducting oxide substrate material for flat panel displays and solar panels [15,16]. The phase studied here, denoted *m*-phase, was first identified using powder X-ray diffraction and solved by a combination of electron diffraction and high-resolution imaging, then later confirmed by neutron diffraction [17]. This phase has a monoclinic unit cell with $a = 11.69\,\text{Å}$, $b = 3.17\,\text{Å}$, $c = 10.73\,\text{Å}$, and $\beta = 99^\circ$. The plane group is p2, and the origin can be defined by fixing phases of two strong reflections that have odd parity and are non-collinear with the transmitted beam. The plate-like structure is shown in Fig. 1.

A two-dimensional electron precession dataset from GITO was captured on a precession system based upon the JEOL 2000FX microscope described elsewhere [18]. Operating conditions were as follows: [0 1 0] projection; 200 kV accelerating voltage; cone semi-angle of 24 mrad ($0.96\,\text{Å}^{-1}$ in the diffraction plane); parallel illumination; 60 Hz precession scan rate; smallest condenser aperture (10 um), and ~50 nm probe size. The dataset (henceforth referred to as "precessed") was captured on a GATAN US1000 CCD. A second dataset was acquired by conventional fine probe diffraction (henceforth referred to as "dynamical") using an identical illuminated region and illumination conditions excepting beam precession, within experimental error, and using identical probe size and exposure times.

Intensity measurements of the digital images were conducted within EDM [19]. The intensities collected from the precession dataset were

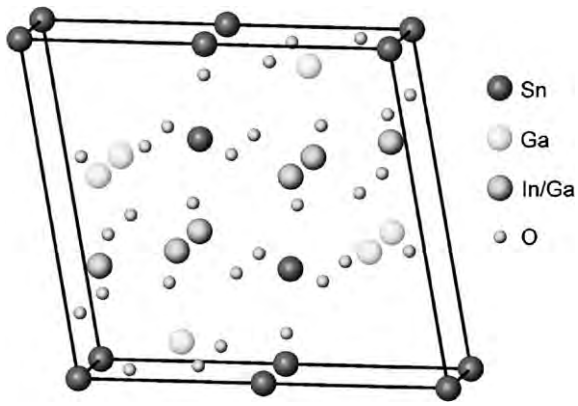

Fig. 1. Structure of $(Ga,In)_2SnO_4$. In/Ga balls represent mixed occupancy sites.

Table 1
Kinematical amplitudes and experimental amplitudes for the GITO precession experiment (normalized to strongest reflection)

h	k	g	F_{kin}	F_{prec}
1	1	0.1162	1.47E-01	6.13E-01*
−1	1	0.1360	1.38E-01	5.21E-01*
2	0	0.1711	2.25E-01	5.46E-01*
2	1	0.1816	3.98E-03	2.75E-01*
0	2	0.1864	8.14E-02	3.41E-01*
1	2	0.1925	1.49E-01	4.50E-01*
−2	1	0.2072	4.52E-01	7.09E-01*
−1	2	0.2169	1.94E-01	6.43E-01*
2	2	0.2325	6.26E-02	4.15E-01*
3	0	0.2566	1.99E-01	3.54E-01
3	1	0.2590	1.69E-01	5.04E-01
−2	2	0.2720	4.92E-03	2.69E-01
1	3	0.2793	2.16E-01	3.19E-01
0	3	0.2796	8.81E-01	7.65E-01
−3	1	0.2864	1.80E-01	3.03E-01
3	2	0.2926	4.21E-04	2.95E-01
2	3	0.3041	6.88E-01	6.61E-01
−1	3	0.3049	1.64E-01	3.51E-01
−3	2	0.3400	1.04E-01	3.84E-01
4	1	0.3403	7.82E-02	2.82E-01
4	0	0.3422	4.63E-02	2.54E-01
3	3	0.3487	2.38E-01	3.17E-01
−2	3	0.3499	1.39E-01	3.95E-01
4	2	0.3631	2.61E-01	5.38E-01
−4	1	0.3684	1.00E+00	1.00E+00
1	4	0.3692	4.51E-03	3.29E-01
0	4	0.3728	3.59E-02	3.30E-01
2	4	0.3851	3.31E-02	2.26E-01
−1	4	0.3953	9.80E-02	3.07E-01
4	3	0.4066	9.76E-02	2.70E-01
−3	3	0.4080	1.69E-01	3.78E-01
−4	2	0.4145	6.71E-02	2.99E-01
3	4	0.4182	1.22E-01	3.70E-01
5	1	0.4233	1.21E-01	2.64E-01
5	0	0.4277	2.22E-01	4.67E-01
−2	4	0.4338	5.70E-01	5.83E-01
5	2	0.4390	1.15E-01	2.89E-01
−5	1	0.4518	1.11E-01	2.32E-01
1	5	0.4604	7.16E-02	2.81E-01
0	5	0.4660	2.62E-02	2.53E-01
2	5	0.4706	8.39E-02	2.87E-01
5	3	0.4730	4.74E-02	2.61E-01
−4	3	0.4745	6.15E-02	2.36E-01
−3	4	0.4845	6.91E-02	2.52E-01
−1	5	0.4868	3.66E-01	3.36E-01
−5	2	0.4926	1.37E-02	2.71E-01
6	1	0.5071	2.49E-02	2.60E-01
6	2	0.5179	3.47E-01	4.36E-01
5	4	0.5216	1.52E-02	2.38E-01
4	5	0.5332	6.38E-02	3.06E-01

Table 1 (*continued*)

h	k	g	F_{kin}	F_{prec}
−6	1	0.5358	3.08E-02	2.39E-01
−4	4	0.5440	3.66E-01	3.82E-01
−5	3	0.5464	2.58E-01	4.11E-01
2	6	0.5586	7.44E-01	5.24E-01
0	6	0.5592	1.65E-01	3.27E-01
−3	5	0.5661	6.60E-02	2.48E-01
−6	2	0.5728	4.36E-01	4.18E-01
3	6	0.5776	6.87E-02	2.31E-01
−1	6	0.5788	1.37E-02	2.39E-01
6	4	0.5853	6.19E-02	2.36E-01
7	2	0.5987	2.08E-01	2.87E-01
7	0	0.5988	5.03E-02	2.94E-01
4	6	0.6082	4.42E-02	2.73E-01
−5	4	0.6098	1.60E-01	2.42E-01
−4	5	0.6198	3.29E-02	2.59E-01
7	3	0.6200	1.45E-02	2.45E-01
6	5	0.6370	4.51E-01	4.14E-01
1	7	0.6446	1.39E-01	2.56E-01
5	6	0.6487	9.06E-02	2.43E-01
−3	6	0.6507	3.08E-02	2.58E-01
0	7	0.6524	1.85E-01	3.54E-01
3	7	0.6626	2.44E-01	2.42E-01
8	1	0.6761	3.75E-01	3.70E-01
−6	4	0.6799	5.63E-02	2.39E-01
7	5	0.6989	1.04E-01	2.38E-01
−7	3	0.6994	3.44E-02	2.69E-01
−2	7	0.6998	5.12E-01	4.44E-01
5	7	0.7220	8.62E-05	2.51E-01
8	4	0.7263	3.11E-01	2.86E-01
−8	2	0.7369	5.04E-01	3.31E-01
1	8	0.7370	1.99E-02	2.64E-01
−6	5	0.7453	4.77E-01	4.18E-01
7	6	0.7527	1.72E-01	2.32E-01
−7	4	0.7532	7.52E-02	3.02E-01
−5	6	0.7553	1.23E-02	2.44E-01
9	2	0.7633	7.26E-02	2.70E-01
−1	8	0.7636	3.23E-02	2.38E-01
−9	1	0.7899	1.37E-01	3.46E-01
2	9	0.8294	3.29E-01	2.90E-01
6	8	0.8364	1.66E-01	3.66E-01
10	1	0.8459	1.52E-01	2.61E-01
4	9	0.8549	2.41E-01	2.45E-01
10	0	0.8554	4.02E-03	2.76E-01
−4	8	0.8676	1.70E-01	2.33E-01
10	4	0.8780	2.78E-01	2.84E-01
−8	5	0.8861	1.76E-01	2.45E-01
−9	4	0.9064	6.00E-02	3.77E-01
−3	9	0.9147	1.20E-01	2.54E-01
1	10	0.9225	1.14E-01	2.52E-01
11	1	0.9310	1.67E-01	2.38E-01
0	10	0.9320	3.48E-01	3.69E-01
−10	3	0.9406	3.05E-01	2.66E-01
−7	7	0.9520	1.67E-01	2.94E-01

Table 1 (*continued*)

h	k	g	F_{kin}	F_{prec}
−6	8	0.9690	2.84E-01	3.52E-01
−2	10	0.9735	2.50E-01	2.70E-01
10	7	0.9913	1.80E-01	2.44E-01
12	3	1.0208	1.64E-01	2.73E-01
12	0	1.0265	2.49E-01	2.91E-01
−12	1	1.0452	2.28E-02	2.31E-01
−10	6	1.0928	4.17E-01	2.63E-01
13	1	1.1013	1.23E-01	2.44E-01
−12	3	1.1053	2.41E-01	2.63E-01
11	8	1.1054	4.00E-02	2.35E-01
4	12	1.1172	1.92E-01	2.74E-01
−4	11	1.1304	3.22E-01	2.60E-01
−1	12	1.1349	3.66E-02	2.56E-01
8	11	1.1401	1.74E-01	2.25E-01
−10	9	1.2883	2.42E-01	2.43E-01
−11	8	1.2887	2.80E-02	2.35E-01
−14	4	1.3088	8.89E-02	2.27E-01
−4	14	1.3997	1.15E-01	2.61E-01

See Fig. 2 for experimental errors. Reflections excluded in direct methods are starred (*).

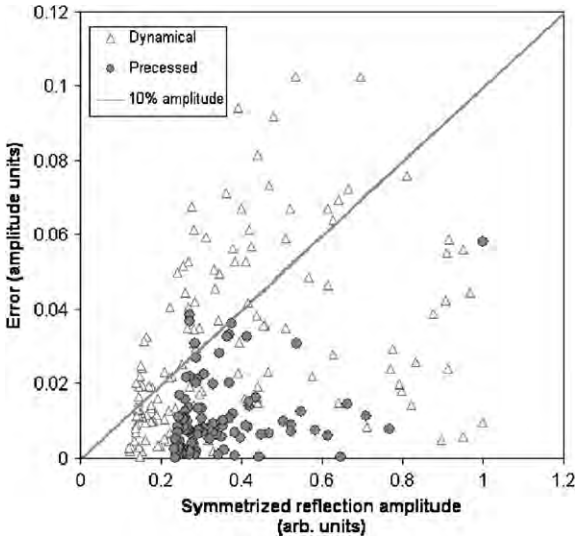

Fig. 2. Friedel errors (amplitudes). Most precession errors (circles) are less than 10% of the amplitude and decrease with increasing amplitude. Non-precessed Friedel errors have more scatter and often exceed 10% of the measured amplitude due to the asymmetric sampling of relrods.

symmetry-averaged and used directly with the fs98 code packaged within EDM. The software uses an accurate cross-correlation algorithm similar to that described by [20] to collect intensities, wherein a unitary spot motif generated by combining reflection profiles is used to quantify the reflection intensities. The precession system was able to bring the diffracted beams down to uniform spots suitable for measurement by this method. 121 symmetry-averaged intensities were collected and their amplitudes are given in Table 1.

Precession decreases error between Friedel pairs, hence a slight mistilt of the zone axis with respect to the incident beam is tolerable for quantitative electron crystallography. For instance, a mistilt of less than one milliradian is readily compensated by a precession cone semi-angle of 20 mrad. This effect is seen in experimental data. Error between Friedel equivalents was evaluated in both precessed and non-precessed diffraction patterns according to the metric,

$$E_{\text{Friedel}} = \frac{|F_g - F_{\bar{g}}|}{2}. \quad (1)$$

The non-precessed ZAP was aligned visually to be as on-zone as possible during the diffraction experiment. Datasets were normalized to the strongest reflection to facilitate a direct comparison, and the errors have been plotted in Fig. 2. The precession data had a higher minimum measurement threshold, indicative of more kinematical behavior since the transmitted beam is stronger in relation to scattered beams (the two datasets had identical exposure times). Fig. 2 shows that the Friedel error in the precession pattern is overall quite low, and excepting the strongest reflection the percentage error decreases as amplitude increases. In contrast, the dynamical dataset errors have a larger scatter, and several error points exceed 10% of the reflection amplitude. This is noteworthy because, the Friedel error in the dynamical pattern was larger than precession even though spots in the non-precessed dataset were isotropically shaped and more peak-like, hence easier to measure than the precession pattern which exhibited residual projector distortions that altered spot profiles asymmetrically.

2. Analysis

The set of kinematical amplitudes computed from the known structure will be used as the reference for this comparison. Key reflections in the experimental precession data with spacings that define the atomic positions (about 0.25–1 Å^{-1}) match the kinematical data well in relative intensity from a qualitative standpoint (see Fig. 3). The experimental pattern contains increased intensity near the transmitted beam and the outer reflections are damped (Fig. 3(b)), owing to a combination of a Lorentz-type geometric contribution [21], Debye–Waller-type radial damping, and typical dynamical behavior where reflections near strong beams are often overemphasized due to strong multiple scattering. The experimental map is especially promising because stronger structural reflections beyond 0.5 Å^{-1}, even though they are damped, still exhibit qualitatively well-correlated intensity ratios.

To better quantify these effects, the datasets were plotted against the kinematical amplitudes from the known structure. Fig. 4 shows symmetrized experimental precession and dynamical datasets normalized to the strongest intensity in each set and reflection amplitudes are coded by symbol in ranges of $g = 0.25\,\text{Å}^{-1}$ within the plots. In order for a pseudo-kinematical interpretation to be applicable, the amplitudes must be approximately linear and ratios between reflections should be preserved. The precession data contains several outlier reflections, primarily at $F_{\text{norm}} \sim 0.2$ (note that this is specific to the [0 1 0] GITO zone axis),

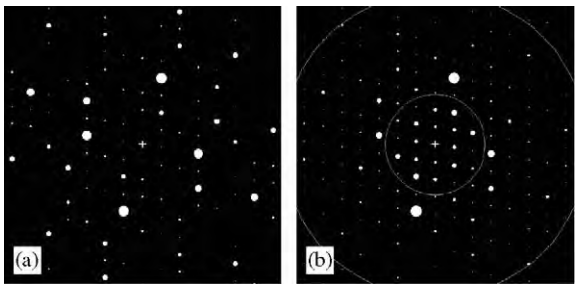

Fig. 3. (a) Kinematical amplitudes and (b) experimental intensities. Annulus describing the range 0.25–0.75 Å^{-1} is bounded by the circles.

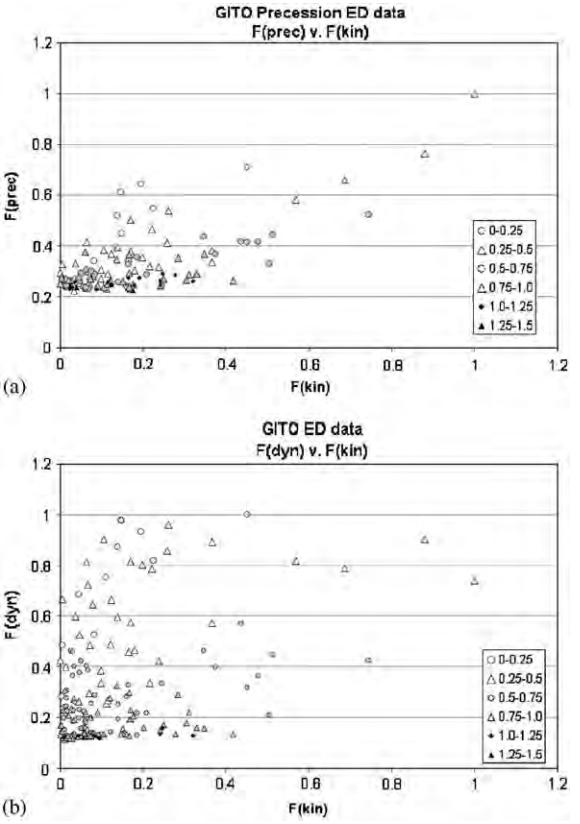

Fig. 4. Experimental precession amplitudes (a) and dynamical amplitudes (b) plotted against kinematical amplitudes calculated from the known structure.

and exhibits a distinctive positive offset of weak reflections whose values are above the measurement threshold. Regardless of the offset, most reflections follow the targeted linear trend, and the precession dataset is distinctly linear in comparison to the dynamical amplitudes of Fig. 4(b), which are hopelessly mixed. The most encouraging aspect of the precession data is that even with inevitable specimen thickness averaging, the outliers are predictable and the amplitudes of structural significance may be interpreted directly.

Raw GITO precession datasets maintain good linearity to $t \sim 200\,\text{Å}$ according to precession multislice simulations (to be discussed in detail in a future paper). As thickness increases, intensity deviations manifest in the reflections at the extremes of the structure-defining reflection range and eventually encroach into the range of

reflections that have strong bearing on the structure, causing direct methods to generate poorer structure maps. Due to the precession geometry, low-index precessed reflections receive considerable coupled intensity from the transmitted beam, thus the reflections of greatest concern are those nearest the transmitted beam that are usually weak for real structures. This behavior suggests that, for unknown structures of moderate thickness, a good starting point is to exclude reflections that fall outside of the structure-defining range of $0.25\,\text{Å}^{-1} < g < 1.25\,\text{Å}^{-1}$. This approach is effective with precession data from GITO crystals to about $t = 750\,\text{Å}$ when 24 mrad precession semi-angle is used. Higher precession semi-angles can improve this to some extent (extending the range by 5–10 nm) but HOLZ overlap with the ZOLZ is likely [22]. Larger thicknesses will certainly require a forward calculation to correct the intensities for multiple scattering, one approach being the two-beam correction employed in the previous study by Gjønnes [14].

The precession dataset with $g < 0.25\,\text{Å}^{-1}$ excluded was employed in a direct methods calculation and produced four unique solutions (shown in Fig. 5(a)). The solution with the clearest peak-like features from the dynamical dataset is given in Fig. 5(c) for comparison. The precession solutions bear near-identical features to each other and demonstrate very well-defined peak locations. Some of the strong scatterers in the structure are weakly emphasized (i.e., the In/Ga columns at 0.35*a*, 0.38*c*), however, all expected atom locations contain atom-like features above the noise floor that would be considered as potential atom locations in an a priori structure investigation. The quality of these solutions, compared with the solution from the dynamical dataset acquired from the identical specimen region, is unmistakable. Fig. 5(c) is typical of a first-try solution with a complex oxide of unknown thickness; it is well-known that bulk oxide structures are as a rule very difficult to solve from TED data alone. In stark contrast to precession, the best dynamical solution only located Sn atoms at the corners and middle of the unit cell, and the central atoms were placed at incorrect positions. Of seven unique solutions

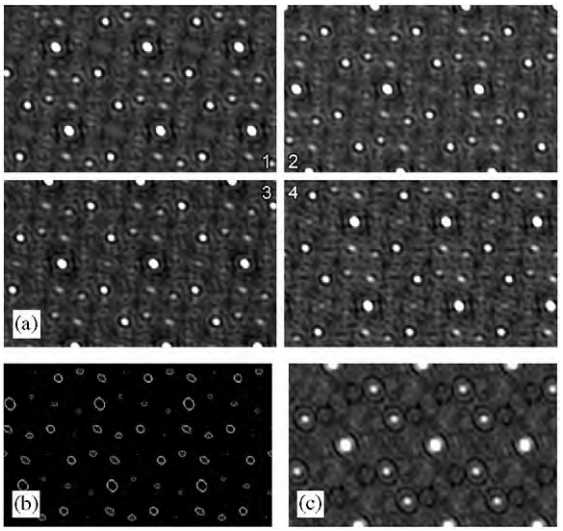

Fig. 5. (a) Four unique DM solutions generated from precession data. Reflections below $g = 0.25\,\text{Å}^{-1}$ were excluded. (b) Topographical map of solution 4. Well-defined peaks above the noise floor correspond to atomic positions. (c) DM solution from dynamical dataset. No high-resolution phases were used to generate these maps.

generated from the dynamical data, only two possessed atom-like features and those solution maps would be untrustworthy unless more a priori information such as phases from high-resolution imaging was available to constrain the calculation.

It is worthwhile to note the effect of thickness averaging on the data as the wedge-shaped illuminated region in the experiments represented a range of thicknesses. As is described elsewhere, the potential function restored by direct methods closely approximates the modulus of the Babinet $|1-\psi(r)|$ [5]. In conventional electron diffraction, aspects of the structure such as the oxygen atoms and heavy cations (manifesting as sharp well-defined features) exchange prominence in the exit wavefunction with increasing crystal thickness due to variation in oscillation periodicities for discrete atomic columns of differing composition. To get projections that faithfully indicate all features of one type (critical for direct interpretability), thin and uniform crystals are required to avoid overlap of oscillations from constituent columns. In the case of GITO, interpretability of the Babinet rapidly diminishes beyond about 30 nm thickness

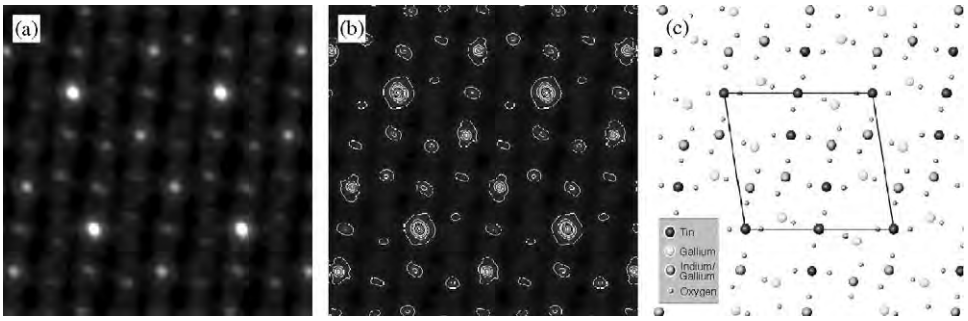

Fig. 6. DM solution from the precession intensities (all reflections included).

as indicated by simulation; accordingly, large thickness variation and small oscillation periodicities render most conventional datasets from GITO intractable a priori by direct methods. Precession data exhibit some insensitivity to thickness averaging, making direct interpretation possible for crystals with varying thickness, especially if some phases are known. The result of Fig. 5 illustrates that PED of moderately thick crystals (<50 nm) with good projection characteristics requires no additional phase information to generate good structure maps.

It has been suggested by Dorset and others to increase contrast of the electron diffraction data by using intensities with direct methods rather than structure factor amplitudes [6,23]. This approach is supported by a two-beam argument, applicable to polycrystal diffraction, texture patterns, and also to precession data (effective integrated two-beam) under some conditions. However, in general a more complete dynamical diffraction analysis is needed which will be discussed in detail elsewhere [24]. From Blackman theory [25], the measured intensity $I_{\mathrm{dyn}}(\mathbf{g})$ is related to the kinematical structure factor $F(\mathbf{g})$ as

$$I_{\mathrm{dyn}}(\mathbf{g}) \sim F(\mathbf{g})^{\alpha}, \tag{2}$$

where the exponent α varies from 2 to 1 as the product of thickness and $F(\mathrm{g})$ increases. For PED on thicker crystals where the structure is unknown, use of intensities approximates a dynamical two-beam correction, which can be used to generate starting structure maps. These may later be refined to generate more accurate correction factors in an iterative correction scheme. The practical effect on the data is a preferential enhancement of strong beams which, if the strong structure-defining amplitudes are nearly correct with respect to each other, emphasizes key structural features above "noisy" weak reflections that can generate ambiguous oscillation maxima in the Fourier synthesis.

Incorporating this alternate approach with the GITO data, the strong structure-defining reflections in the 0.25–0.5 Å region become more prominent as the contrast between strong and weak beams is enhanced. The resulting map (Fig. 6(a) and (b), where all measured reflections were included in DM) more clearly shows atom-like features at all expected cations location due to attenuation of noisy reflections. Peak locations from the intensities-derived map are consistent within a few picometers to those found from using amplitudes with low-g reflections excluded (Fig. 5). The cation positions measured from the amplitudes-derived map (unrefined) are given in Table 2. HREM and neutron-refined GITO atom positions from Sinkler et al. [17] are reproduced for comparison, showing good correspondence with precession results. Precession-derived maps without subsequent refinement result in column positions located on average within 4 picometers of the neutron-refined positions.

3. Conclusions

The success of direct methods is highly dependent upon key constraints; given a nearly kinema-

Table 2
Atom positions from HREM, neutron diffraction (refined), and unrefined positions from precession

	HREM		Neutron		Precession		Displacement (Å)	
	x	z	x	z	x	z	ΔR_{HREM}	$\Delta R_{\mathrm{Neutron}}$
Sn1	0.0	0.0	0.0	0.0	0.0	0.0	0.0	0.0
Sn2	0.515	0.062	0.5	0.0	0.5	0.0	0.474615	0.0
Sn3	0.594	0.320	0.5918(6)	0.3112(7)	0.585113	0.312169	0.017950	0.0065(5)
In/Ga1	0.305	0.360	0.3281(6)	0.3859(7)	0.345947	0.379929	0.275989	0.0516(5)
In/Ga2	0.078	0.328	0.0756(8)	0.3053(9)	0.079877	0.305699	0.057683	0.0023(7)
Ga1	0.172	0.672	0.1500(5)	0.6022(6)	0.172498	0.602720	0.552591	0.0684(8)
Ga2	0.234	0.031	0.2624(5)	0.0869(5)	0.232436	0.078043	0.255026	0.1217(5)

Precession results match very closely with the neutron-refined positions.

tical dataset, DM will generate potential maps that closely match the true solution. Electron precession demonstrates the ability to linearize the GITO dataset to a kinematical approximation allowing nearly direct interpretation. The experimental precession data from GITO is linear in the regime where the structurally important reflections are located, and appears to be much less sensitive to the variations in thickness that prove debilitating for conventional electron diffraction datasets. The results also suggest a systematic behavior to the data errors present, and excluding overemphasized reflections in precession datasets that have little bearing on the structure is a suitable starting strategy. A comprehensive understanding of these errors in relation to thickness and illumination conditions is necessary to allow general use of precession data in a completely pseudo-kinematical capacity; however this study shows that in certain cases the data will be directly usable without modification.

Acknowledgements

Funding for this project was provided by UOP LLC, STCS, DOE (Grant no. DE-FG02-03ER 15457), and the Fannie and John Hertz Foundation.

References

[1] L.D. Marks, W. Sinkler, Micros. Microanal. 9 (2003) 399.
[2] B. Kabius, M. Haider, S. Uhlemann, E. Schwan, K. Urban, H. Rose, J. Elec. Micros. 51 (2002) S51.
[3] P.D. Nellist, M.F. Chisholm, N. Dellby, O.L. Krivanek, M.F. Murfitt, Z.S. Szilagyi, A.R. Lupini, A. Borisevich, W.H. Sides, S.J. Pennycook, Science 305 (2004) 1741.
[4] W. Sinkler, L.D. Marks, J. Micros. 194 (1999) 112.
[5] W. Sinkler, E. Bengu, L.D. Marks, Acta Crystallogra. A 54 (1998) 591.
[6] T.E. Weirich, Cryst. Rep. 49 (2004) 379.
[7] C.S. Own, A.K. Subramanian, L.D. Marks, Micros. Microanal. 10 (2004) 396.
[8] C.J. Gilmore, L.D. Marks, D. Grozea, C. Collazo, E. Landree, R.D. Twesten, Surf. Sci. 381 (1997) 77.
[9] J. Jansen, D. Tang, H.W. Zandbergen, H. Schenk, Acta Crystallogra. A 54 (1998) 91.
[10] J.M. Zuo, M. Kim, M. O'Keeffe, J.C.H. Spence, Nature 401 (1999) 49.
[11] R. Vincent, P.A. Midgley, Ultramicroscopy 53 (1994) 271.
[12] J. Gjønnes, V. Hansen, B.S. Berg, P. Runde, Y.F. Cheng, K. Gjønnes, D.L. Dorset, C.J. Gilmore, Acta Crystallogra. A 54 (1998) 306.
[13] M. Gemmi, X.D. Zou, S. Hovmoller, A. Migliori, M. Vennstrom, Y. Andersson, Acta Crystallogra. A 59 (2003) 117.
[14] K. Gjønnes, Y.F. Cheng, B.S. Berg, V. Hansen, Acta Crystallogra. A 54 (1998) 102.
[15] D.D. Edwards, T.O. Mason, W. Sinkler, L.D. Marks, K.R. Poeppelmeier, Z. Hu, J.D. Jorgensen, J. Solid State Chem. 150 (2000) 294.
[16] J.H. Hwang, D.D. Edwards, D.R. Kammler, T.O. Mason, Solid State Ionics 129 (2000) 135.
[17] W. Sinkler, L.D. Marks, D.D. Edwards, T.O. Mason, K.R. Poeppelmeier, Z. Hu, J.D. Jorgensen, J. Solid State Chem. 136 (1998) 145.
[18] C.S. Own, L.D. Marks, W. Sinkler, Rev. Sci. Instrum. 76 (2005).
[19] R. Kilaas, L.D. Marks, C.S. Own, Ultramicroscopy 102 (2005) 233.

[20] P. Xu, G. Jayaram, L.D. Marks, Ultramicroscopy 53 (1994) 15.
[21] K. Gjønnes, Ultramicroscopy 69 (1997) 1.
[22] C.S. Own, L.D. Marks, Micros. Microanal. (submitted).
[23] D.L. Dorset, Structural Electron Crystallography, Plenum Publishing Co., New York, 1995.
[24] C.S. Own, Sinkler, W., Marks, L.D., (in preparation).
[25] M. Blackman, Proc. R. Soc. London, A 173 (1939) 68.